When cells respond to light

All you need is LOV

Van Geel, O.

Publication date
2020
Document Version
Other version
License
Other

CHAPTER 2

Increasing spatial resolution of photoregulated GTPases through immobilized peripheral membrane proteins

Orry Van Geel[1], Roland Hartsuiker[1] & Theodorus W. J. Gadella[1]

[1]Swammerdam Institute for Life Sciences, Section of Molecular Cytology, van Leeuwenhoek Centre for Advanced Microscopy, University of Amsterdam, Science Park 904, 1098 XH Amsterdam, The Netherlands.

Accepted in Small GTPases, 2018

Abstract

Light-induced dimerizing systems, e.g. iLID, are an increasingly utilized optogenetics tool to perturb cellular signaling. The major benefit of this technique is that it allows external spatiotemporal control over protein localization with sub-cellular specificity. However, when it comes to local recruitment of signaling components to the plasmamembrane, this precision in localization is easily lost due to rapid diffusion of the membrane anchor. In this study, we explored different approaches of countering the diffusion of peripheral membrane anchors, to the point where immobilized fractions could be detect with iFRAP on a timescale of several minutes. One method involves simultaneous binding of the membrane anchor to a secondary structure, the microtubules. The other strategy utilizes clustering of the anchor into large immobile structures, which can also be interlinked by employing tandem recruitable domains. For both approaches, the anchors were peripheral membrane constructs, which also makes them suitable for *in vitro* use. Upon combining these slower diffusing anchors with recruitable guanine exchange factors (GEFs), we show that we can elicit much more localized morphological responses from Rac1 and Cdc42 as compared to a regular CAAX-box based anchor in living cells. Thanks to these new slow diffusing anchors, more precisely defined membrane recruitment experiments are now possible.

Introduction

Plasma membranes (PM) are hotspots for cellular signaling[1,2] since they represent the interface of cells with their extracellular environment. Signaling pathways triggered at the PM contain a variety of effector proteins that can become temporarily associated with the PM, often through the involvement of lipid binding domains[3]. Recently it became possible to gain control over the translocation process to the PM with unprecedented precise spatial and temporal control through optogenetics[4,5]. This technique relies on incorporating light-sensitive protein domains in such a way that protein binding sites can become blocked or available, depending on the light-induced conformational state of these domains[5,6].

Signaling through Rho-GTPases is often studied with perturbation methods[7] of which optogenetics provide several advantages. For example, the iLID optogenetic system, has previously been used in combination with CAAX lipidation to locally target Rho-GTPase signaling and induce morphology changes by Guntas et al. They achieved local activation of these GTPases by translocating Dbl homology (DH)/pleckstrin-homology(PH) domains of guanine exchange factors (GEFs) specific to Rac1 and Cdc42, namely Tiam1 and ITSN1 respectively. Branching of the actin cytoskeleton and the formation of lamellipodia was induced through Rac1 activation. Active Cdc42 should mainly lead to bundled actin and filopodia, but activated Cdc42was also observed to induce lamellipodia, most likely due to cross-talk of the GTPase pathways[8].

Many different studies have successfully addressed cortical Rho-GTPase signaling with light-induced translocation approaches[9-11]. However, we believe that the spatial confinement of these experiments could be improved further by utilizing constructs with slower diffusing membrane binding domains. In most studies, the membrane anchoring molecules contain some version of a posttranslational prenyl-tail for insertion in the plasmamembrane. Unfortunately, these molecules display high lateral diffusion speeds of about 1µm^2/s [12,13]. This rapid diffusion combined with their relatively low dissociation half-life of 7-10min[14] results in substantial spreading across the PM for any domain attached to these anchors. AsLOV2-based optogenetic tools are among the most commonly used and they normally display a reversion time of around 30s [15], which is sufficient for rapid lateral diffusion to generate relatively wide gradients of light-induced activity outside of the originally illuminated area. This is fine for mimicking cellular responses to wide extracellular gradients, but some signals are initiated on a much more precise scale, e.g. GTPase activity induced at the point of physical contact with the extracellular matrix[16]. A recent study already addressed this spatial confinement problem by comparing different optical dimerizers, and they show that faster switching kinetics are better for maintaining local recruitment[17]. While true, fast kinetics should not be a requirement as this can limit experimental approaches. On top of that, the most common light-responsive domains do not even possess kinetics fast enough to overcome the scattering of activated molecules by lateral diffusion of the traditional membrane anchors to which they are attached.

In order to improve the spatial resolution of light-induced translocation to the PM, we focused on finding a membrane targeting approach with as little diffusion as possible. We did not employ transmembrane domains in view of possible future applications where optogenetics is being combined with emerging *in vitro* technologies[18,19], for which easy purification and reconstitution is important. Therefore, we focused on options that are optimal for both *in vivo* & *in vitro* studies by using peripheral membrane proteins that are not posttranslationally modified. More specifically, we chose the C2 lipid binding domain of lactadherin, which binds phosphatidylserine independent of cofactors[20]. Through fusions of this C2 domain with oligomerizing- or other binding domains, we identified two new membrane anchor constructs with a large immobile fraction on the timescale of asLOV2 kinetics. We show here that these new anchors can be used to elicit a more localized cellular response from light-inducible dimer systems, as compared to the conventional prenylated membrane anchors.

Results

Identifying slow diffusing recombinant membrane affinity tags

In order to create slow diffusing membrane anchors, we evaluated the diffusion rate of several targeted protein fusions (Fig1A-D). Diffusion was analyzed from inverted Fluorescence Recovery After Bleaching (iFRAP)[21] by comparing the relative rates of fluorescence intensity decay, which represent the fraction of anchors that moves outside the targeted ROI. Hence, slower decay points to less lateral diffusion of the anchor. We found that even a single C2 domain initially loses significantly less intensity than the commonly used prenylated protein domains such as KRas4B CAAX-motifs (Fig1E). Next, we examined the effect of tandem C2-domains to create multiple binding sites (Fig1B). We observed the intensity decay, and hence diffusion, slow down with every extra domain (Fig1E). However, the effect is moderate, suggesting that another approach was needed for a bigger impact on diffusion. We speculated that by binding two different structures simultaneously, movement of the anchor would be further restricted, for instance by creating a construct with affinity for both the PM and microtubules (MT). To that end we fused a plus-end-tracking protein, End Binding 3 (EB3), to the N-terminus of a double C2 domain, termed EB3-2C2 from here (Fig1C). The iFRAP data from this fusion protein still displayed fast initial fluorescence decay, but over time this decay slows down after which a plateau is reached at which half the initial intensity remains (Fig1E). This indicates the presence of a substantial fraction of highly immobile molecules. In contrast, we observed how either EB3 or tandem-C2 alone lose almost all of their initial fluorescence within 6min during iFRAP experiments (Fig1F-G). Importantly, that is not the case when they are fused together, which demonstrates that the immobilization of EB-2C2 is greater than its parts (Fig1H). This clearly shows the benefit of double-affinity anchors, although the forced interactions between two structures and possible effects on their function will have to be taken into consideration. Alternatively, we tried slowing down diffusion by increasing the total size by introducing an inducible clustering function. Hence, we tried fusing a tandem C2 to CRY2clust, which homo-oligomerizes upon blue illumination[22], termed CRY2-2C2 from here (Figure 1D). We found that the addition of CRY2 resulted in a slower decay of fluorescence which almost reaches a plateau eventually, just as with EB3-2C2 (Fig1E). An overview of extrapolated numerical values from all iFRAP experiments can be found in Table1. Movement of CRY2-2C2 is reduced almost as much as EB3-2C2, with the former reaching the halftime approximately four times slower and the latter five times slower as compared to standard CAAX lipidation (Table1).

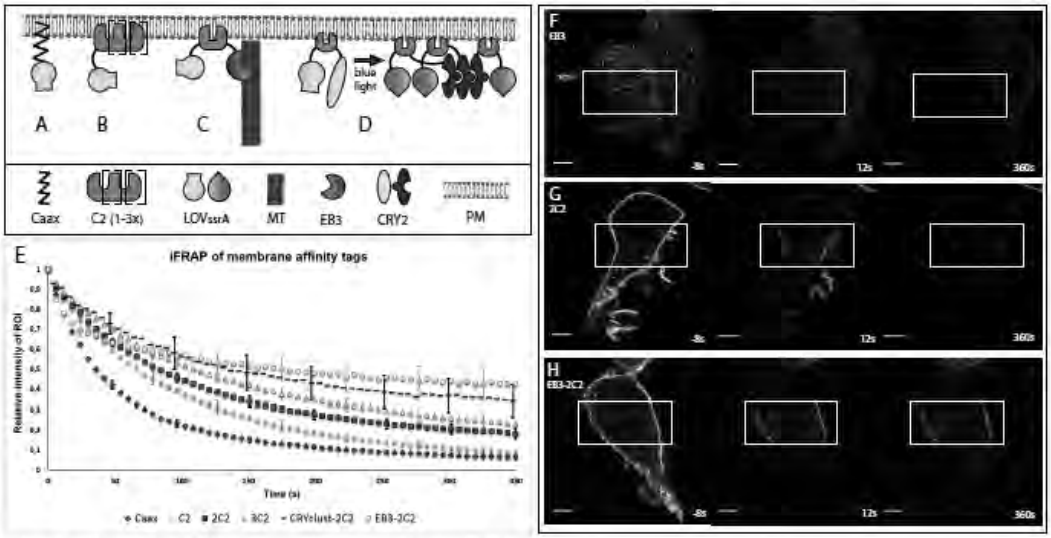

Fig.1. Identifying slow diffusing recombinant membrane affinity tags. (A-D) Schematic overview of all explored membrane targeting strategies for iLID constructs: (A) KRas4B CAAX motif, (B) 1-3x tandem lactadherin-C2 domain, (C) EB3-2xC2 fusion which links PM & MTs (D) CRY2clust-2xC2 fusion which can reversibly cluster. (E) Relative intensity decay from iFRAP experiments plotted over time (n=5). All membrane anchors were tagged with eGFP. Entire cells were bleached with 488nm laser pulses every 8s except within a 13µm square ROI of which the intensities were followed over time. Higher intensity values correspond to lower diffusion rates outside of the targeted ROI. Error bars represent the standard deviation. (F-H) Confocal images of iFRAP experiments with repeated 12s bleach pulses every minute to the entire cells except within the ROI's, here 13 by 26 µm to better visualize the effects. The EB3-2C2 fusion is seen to have much higher residual intensity after 6min then EB3 & 2C2 combined. Scale bars are 5 µm. All experiments were performed in HeLa cells.

Lowering diffusion of membrane anchors through crosslinking

Since our goal is to make optogenetic translocation more local, we also explored ways of decreasing diffusion rates relying on the second, recruitable component (Fig2A-C). We used the iLID system as a representative of translocation modules, and looked at how its recruitable sspB domain could be utilized to alter diffusion. We suspected that by recruiting tandemly repeated sspB domains we can link several peripheral membrane proteins together to create a bigger, less mobile complex (Fig2A), which we again analyzed with iFRAP. When applied to regular CAAX-anchored iLID molecules, we see that one or none sspB domains makes no difference but tandem sspB repeats clearly display slower diffusion (Fig2D). With three or more sspB domains little to no further decrease in diffusion speed was observed (not shown).

Next we attempted to increase the amount of anchors that can be interlinked by having two iLID-ssrA domains on one single membrane anchor, termed 2iLID-2C2 from here (Fig2B). When paired with a single sspB domain this anchor offers no improvement but with a tandem sspB we see a clear initial decrease in diffusion (Fig2E). We also tried to combine the tandem sspB domains with

the cluster forming CRY2-2C2 (Fig2C). Once again, we see no improvement with a single sspB domain, but we do see a clear decrease in diffusion speed when tandem sspB domains are used (Fig2E). This effect also persists over time unlike with 2iLID-2C2. Altogether these results indicate that two sspB domains in tandem are sufficient and proficient at further decreasing lateral diffusion through increasing the total size. This is especially true when combining tandem sspB domains with CRY2-2C2. This construct even outperforms the EB3-2C2 anchor with more than a 50% change in halftime of intensity decay (Table1).

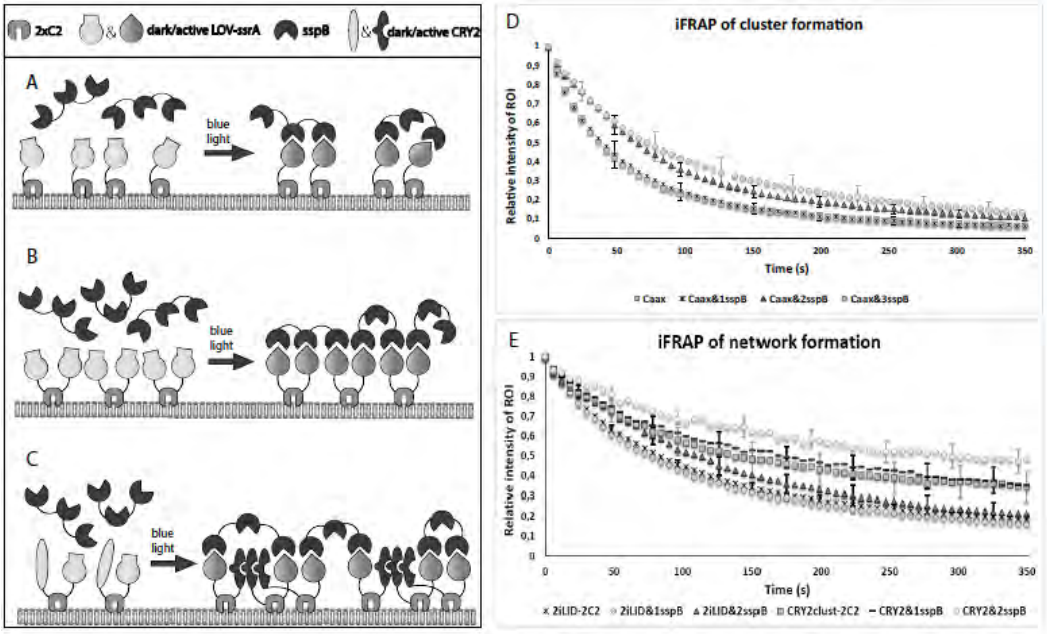

Fig.2. Lowering diffusion of membrane anchors through crosslinking. (A-C) Schematic overview of crosslinking strategies using the ssrA & sspB binding partners of the iLID system: (A) tandem repeated sspB's can cluster membrane-targeted ssrA molecules, (B) tandem sspB's combined with tandem ssrA's can be crosslinked to form big networks of unlimited size in theory, (C) clustering ssrA & crosslinking the clusters with tandem sspB's can also form big networks that can more rapidly grow in size. (D-E) Relative intensity decay from iFRAP experiments plotted over time (n=5). All membrane anchors were tagged with eGFP. Entire cells were bleached with 488nm laser pulses every 8s except within a 13um square ROI of which the intensities were followed over time. Higher intensity values correspond to lower diffusion rates outside of the targeted ROI. Error bars represent the standard deviation. (D) Influence on diffusion of tandem repeated sspB's crosslinking single ssrA's. (E) Influence on diffusion of tandem repeated sspB's crosslinking constructs with multiple ssrA's. All experiments were performed in HeLa cells.

Table1. Overview of relative diffusion rates from iFRAP data.

Construct	Avg halftime (s)*	Intensity after 5min*
CAAX-iLID	35 ± 4	7% ± 1
CAAX + 1sspB	38 ± 6	7% ± 2
1xC2-iLID	63 ± 7	10% ± 3
CAAX + 2sspB	69 ± 10	12% ± 4
CAAX + 3sspB	68 ± 12	16% ± 8
2xC2-iLID	76 ± 9	20% ± 5
2xiLID-2C2 + 1sspB	76 ± 10	18% ± 3
3xC2-iLID	106 ± 14	25% ± 6
2xiLID-2C2 + 2sspB	108 ± 22	23% ± 9
CRY2-2C2	136 ± 34	37% ± 9
CRY2-2C2 + 1sspB	155 ± 32	38% ± 10
EB3-2C2	173 ± 40	44% ± 12
CRY2-2C2 + 2sspB	288 ± 61	48% ± 11

*Data are mean values ± 95% C.I., where n=5 minimally for each condition. Statistically significant differences of the mean halftime or the remaining intensity after 5min can be easily deduced by the presence or absence of overlap in the inferred 95% confidence interval of the corresponding mean values.

Optogenetic characterization of new membrane localization strategies

Now that we identified two different strategies for immobilizing membrane affinity tags, we can characterize their performance in optogenetic translocation experiments. As expected, the type of anchor does not change the properties of the iLID system itself as all of them can display clear translocation to the membrane (Fig3A-C). The only notable difference under our experimental conditions is that the regular CAAX motif shows higher expression levels compared to our new anchors since these are much bigger than CAAX. As a result, more sspB's can bind per area, which results in clearer labeling of the PM (Fig3A). However, such overexpression is rarely required for experiments. The kinetics of the iLID system also remain unchanged when used with a single sspB domain. In contrast, we did observe a delay in the recovery of fluorescence intensity within the cytoplasm when tandem sspB domains are used (Fig3D), pointing to the dissociation speed becoming slower. Probably, this is a result of the stochastic reversion kinetics of asLOV2, which usually occur within a range of 30-50s [9]. Therefore, the dissociation speed depends on the slowest one to revert when tandem sspB's are bound to different LOV domains. As the slower

diffusion from 2sspB seems to come with slower dissociation, we wanted to make sure that the effect on diffusion is dominant enough to prevent spreading of the translocated sspB's outside the illuminated regions. We therefore paired 2sspB with different anchors and activated them within square ROI's of the same size in order to compare the locality of translocation over time. By marking all intensities above the mean value within the ROI at t=0s after subtracting the baseline intensity, we defined the minimal area to which the translocated molecules diffuse. This revealed how the CAAX motif shows moderate local recruitment initially, and that they quickly diffuse over a region nearly twice the size of the targeted ROI (Fig3E). In contrast, both our new anchors kept the translocated sspB's almost entirely within the ROI (Fig3F-G). From this we can conclude that our new membrane anchor approaches pair well with optogenetics and should allow more precise control over local cellular signaling.

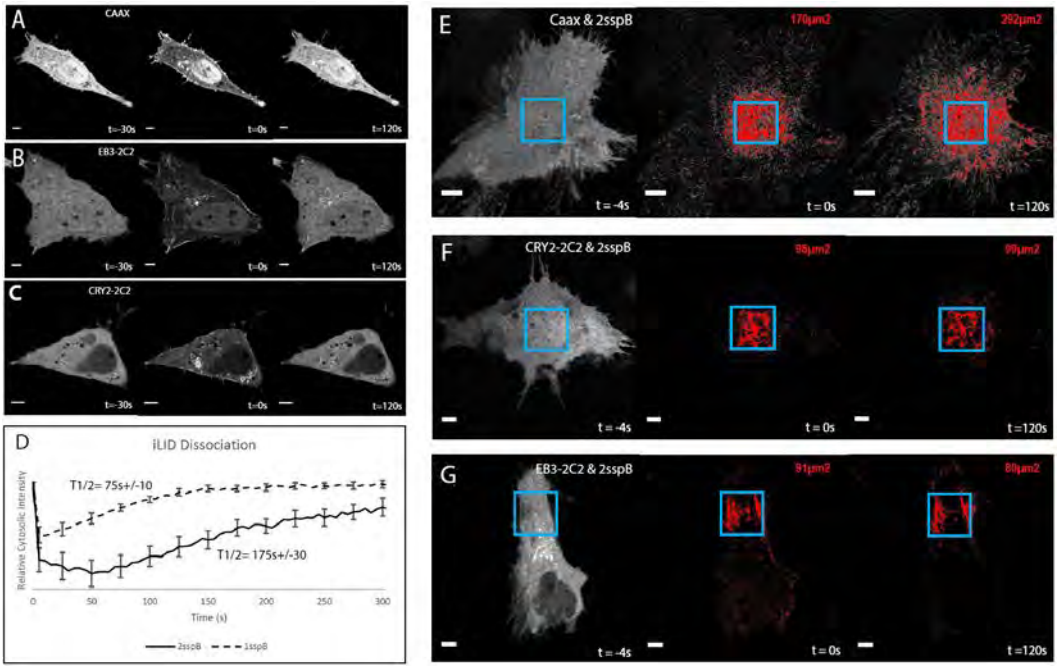

Fig.3. Optogenetic characterization of new membrane localization approach. (A-C) Confocal images showing reversible iLID translocation with different membrane localization tags. Entire cells were illuminated with one single 5s pulse of a 470nm LED at t=0. Scale bars represent 5µm. (D) Dissociation speed of iLID dimerization of single and tandem sspB's was approximated by plotting the recovery of fluorescence in the cytoplasm after an activation pulse of 5s from a 470nm LED was given (n=5). (E-G) Confocal images depicting the spread of locally translocated tandem sspB's. The contrast of translocated sspB molecules was improved by subtracting the baseline intensities from the first image. Activation occurred through 5s pulses of 488nm laser light every 20s within the 13x13µm ROI's indicated in blue. Intensities above the mean value within the ROI's at t=0s are highlighted in red to compare the amount of lateral diffusion. Scale bars represent 5µm. All experiments were performed in HeLa cells.

Application of slow diffusing membrane anchors in manipulating Rho signaling

In order to test whether our new membrane targeting constructs can positively affect the locality of cellular responses from light-induced targeting, we compared recruiting DHPH domains with the standard CAAX motif anchor to recruitment with our new PM anchors. The CAAX construct was paired with a single recruitable domain as in most standard experiments, while our anchors were combined with a tandem recruitable domain to maximize the immobilization of the proteins. We observed clear morphological responses with all the different membrane anchors upon translocating the DHPH domains of Tiam1 and ITSN1 due to alterations of the actin network triggered by these GEFs (Fig4A-B). However, optogenetic activation of the system with the CAAX anchor also resulted in membrane protrusions originating from relatively far outside the ROI. We observed these distant protrusions much more often and pronounced than with the CRY2-2C2 or EB3-2C2 anchor. This already suggests that altered diffusion rates can impact the emergence of these localized membrane deformations. In the case of EB3-2C2, about 1 in 10 cells are unresponsive to localized GEF targeting. This might be due to the fact that proper binding of this PM anchor relies on the presence of MT moving along the PM which can result in certain areas being devoid of a double bound anchor.

In order to quantify the morphological effect, we determined the relative amount of membrane deformation as the ratio of protrusion area over the total cell area, and subsequently identified how much of these protrusions remain strictly within the illuminated ROI. We plotted these values along with their average and 95% confidence interval and found that cells with a CAAX anchor mostly have around one third of the total protrusion area occurring within the region where GEFs where translocated (Fig4C-D). The EB3-2C2 anchor already performs much better with more than half of the protrusion surface located within the ROI. However, the CRY2-2C2 anchor outperforms them all, since the amount of membrane deformation which remains inside the ROI is almost doubled as compared to the caax control (Fig4C-D). From this data we infer that the targeting location of GEFs are better correlated to the induced membrane deformations with lower lateral diffusion rates, thus slower diffusion of membrane anchors can result in more precise optogenetic control over cell signaling and can cause more localized cellular responses.

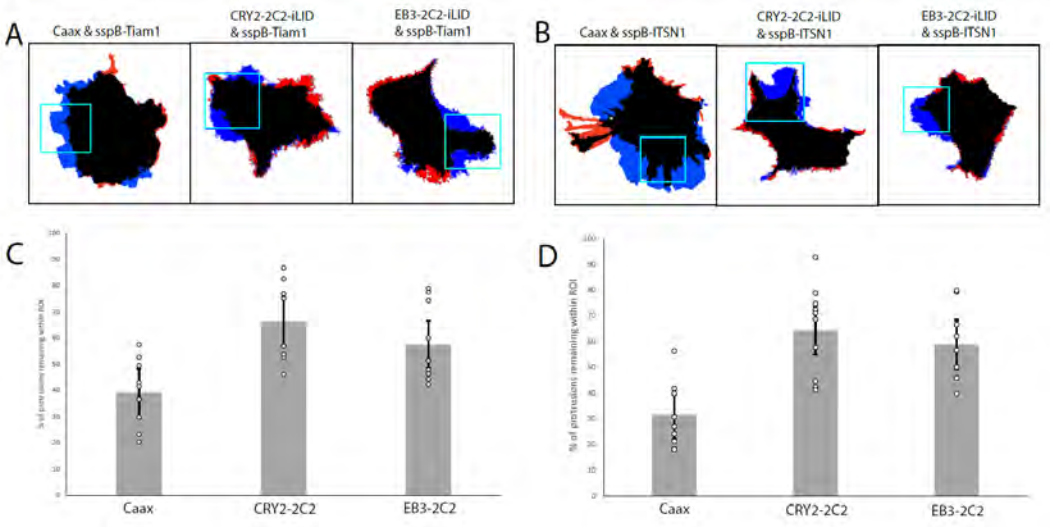

Fig.4. Applications of slow diffusing membrane anchors. (A-B) Local translocation of GEFs to induce membrane deformation. Repeated 5s pulses of 488nm light were given every 20s within the ROI's indicated in light blue. Protrusions after 5min are indicated in dark blue while retractions are indicated in red. (C-D) 95% confidence intervals depicting the percentage of protrusions after 5min that originated from within the ROI's for Tiam1 (C) and ITSN1 (D) translocation (n=10). All experiments were performed in HEK293T cells.

Discussion

The diffusion rate of membrane anchors is often not considered in experiments involving local light induced translocation to the PM. In order to strictly maintain locality, no significant movement of the membrane anchor should occur within the timeframe required for the optogenetic domains to revert to the dark state. The cycling kinetics of the light-sensitive domain is one important factor that determines the extent of unwanted lateral movement[17]. These kinetics can often be altered through point mutations, e.g. the reversion time of the asLOV2 domain can be decreased to a 2s cycle[23]. However, this approach would require continuous local illumination. On top of that, a reversion time of 2s will still allow fast diffusing CAAX-based anchors to disperse the recruited proteins up to 1µm/s outside of the target ROI[12,13]. It would therefore be preferred to slow down diffusion of the membrane anchor instead. We were able to achieve this with two new approaches and show that they induce less spreading of translocated proteins and offer more localized optogenetic control over signaling pathways.

We analyzed the diffusion of membrane anchors with iFRAP[21], because this technique represents diffusion based on all the different binding states that fusion proteins can have. On the other hand, measurements from regular FRAP would be dominated by the diffusion rate of the fastest moving fraction[24]. In our search we first created tandem C2 lipid binding domains and observed a nonlinear decrease in diffusion speed per extra domain (Fig1E). According to the Saffman-Delbruck equation, diffusion scales with the inverse of the radius[25]. Therefore the mobility would decrease when adding more domains. The multiple domains also create extra membrane-binding interactions, thereby lowering the overall dissociation rate, though less impactful with each extra domain. Further improvements were then made by introducing an extra EB3 domain to the anchor which allows crosslinking the PM to microtubules. EB3 has a high affinity for MT +TIPs, but EB3 also displays some affinity for the MT lattice[26,27]. Since the MT lattice is more stable, it would allow the EB3-2C2 double binding to have a large immobile fraction on a timescale of several minutes (Fig1E). The fast moving initial fraction likely reflects partial binding to only a single binding site. The double bound fraction is more restricted in motion because its two dimensional movement is reduced to a semi fixed spot. We believe this membrane binding method could potentially be applied to structures other than MTs, as long as they reside near the PM.

The requirement of a secondary structure for a double anchoring strategy may not always be ideal. Thus, for experiments where EB3-2C2 cannot be used, we developed the CRY2-2C2 anchor, which lowers the diffusion rate by increasing the total size through homo-oligomerization. The same wavelength for activating the LOV domain can be used to induce CRY2clust oligomerization[22]. Hereby clustering will only occur at targeted ROI's and any possible interference with intrinsic functions at the PM will be minimized. In combination with a tandem recruitable component like two sspB domains, it becomes possible that one of these recruited molecules binds two different clusters of CRY2-2C2. Every crosslinking event adds an entire new cluster to the total size, which has a significant impact on diffusion (Fig2E). When using more than two tandem sspB domains, we observed a concomitant reduction in expression level (not shown). Similar problems have been observed for other optogenetic recruitable domains[28]. We therefore picked the double sspB construct as the best one for practical applications.

As expected, we found that combining the new PM anchors with the iLID system[9] did not alter the LOV domain's kinetics compared to the original version with a CAAX motif. Our approach of fusing the iLID domain to the C-terminus of the anchor does not alter the optogenetic domain. Therefore this approach should be compatible with other light-inducible dimerization systems. In combination with a tandem sspB, the dissociation half-time of this recruitable component increases about twofold due to the extra binding site (fig3D). If crosslinking with tandem sspB's is required along with fast on/off kinetics, then a range of point mutations[15] can still be introduced to the light-sensitive domain of choice in order to counteract this increased dissociation effect.

So far, local translocation experiments have ignored the diffusion rate of membrane anchors, since local effects can still be achieved if the targeting ROI is kept small enough to allow for some spreading[8,9]. The problem here is that there is no control over the amount of spreading. In order to end up with a similar local effect, increased expression levels and higher illumination frequencies are required as compared to a system where diffusion is not a factor. However, the expression levels of recruitable proteins should be kept as low as possible in order to prevent a shift in equilibriums of enzyme activities due to overexpression, which may cause pre-activation of the system and trigger subsequent downstream effects[29-31]. In the case of GTPase signaling, it has been known for a while that their activities can be highly localized[16,32]. Hence, experiments with unnecessary wide gradients of translocated GEFs cannot mimic these intrinsic localizations precise enough. For instance, endogenous Rac1 recruitment is dependent on asymmetric phospholipid distribution and forms distinct local clusters[33]. These clusters will display restricted diffusion due to interactions with transmembrane proteins, e.g. TMEM8A[34].

Since the recruited GEFs are unregulated constitutively active mutants[9-10], fast diffusing recruited GEFs can drift far outside their recruited area before encountering and activating a target GTPase. By contrast, endogenous GEFs will interact with a plethora of regulating proteins[35], which most likely contribute to restricting their diffusive motion and thereby keep their activity localized. In order to mimic this situation, it is required that the artificially recuited GEFs display a similar restricted motion. It should be realized that the use of our membrane anchors together with light-induced dimerization is of course an artificial system. Hence, care should be taken in interpreting results towards the biologically relevant endogenous situation. The advantage of optogenetic activation is that no upstream signaling is activated such as receptors or heterotrimeric G-proteins. Thereby the activation of small GTPases directly downstream of the GEFs can be studied in isolation. The better immobilized anchors in combination with optogenetics can mimic the situation where GTPases are activated in a spatially confined way. In that respect, we find that our new tools may be specifically relevant for the future study of GTPases during specific processes such as trans-endothelial migration (TEM). For instance, SH3-containing GEF binding to Intercellular Adhesion Molecule 1 (ICAM-1) clusters, leads to spatially confined RhoG activation and ultimately promotes TEM[36,37]. This process of clustering and local activation can be mimicked with our light inducible oligomerizing CRY2-2C2 anchor. Likewise, processes where the freedom of motion is reduced from 2D to a semi 1D situation might be mimicked with the EB3-2C2 anchor, e.g. when the GEF called Trio gets activated while it simultaneously interacts with ICAM-1 within the PM and with the actin cytoskeleton through filamin[36,38].

The new membrane anchors with much larger immobile fractions should be the preferred anchor choice for experiments that mimic cellular signaling on very small scales. Our proof-of-concept experiment of recruiting Tiam1 and ITSN1 with the new anchors already revealed a close correlation between GEF localization and membrane deformation (Fig4), which implies that small

scale direct interactions of downstream components are sufficient to induce lamellipodia. Direct interactions between Tiam1 and Arp2/3, Rac1, WAVE have been identified already[39,40]. Our data further suggest that a temporary and spatially confined complex is formed with these components that might be instrumental in reorganizing the actin cytoskeleton.

We focused on improving the spatial resolution for optogenetic translocation experiments, however the slow diffusing anchors can also be utilized in combination with other tools that can be used for local control of cell signaling. For instance, the increasing number of photoactivatable proteins that have become available[41,42] will exhibit fast diffusion rates while untethered, but fused to the new PM achors their activity will mostly be confined to targeted areas only. By choosing to work with peripheral membrane proteins, the new constructs require no post-translational modification and hence should allow easy purification for *in vitro* experiments. Since artificial membranes are normally less crowded than PMs, it then becomes even more important to have rather immobile membrane anchors if similar levels of locality as *in vivo* are required. Our PM anchors should make it possible now to explore localized effects of isolated proteins when translocated to the membrane of *in vitro* structures like droplets or liposomes.

With two new approaches of slowing down diffusion from membrane affinity tags, we expand the ever-growing optogenetic toolbox with new ways of increasing the spatial resolution at the PM with these light-inducible systems. One way by utilizing double differential binding spots, the other through induced clustering of the anchor. Both of these will allow small scale signaling events to be mimicked much more closely and should result in more precise future optogenetic experiments.

Materials & Methods

Plasmid constructs

Lactadherin-C2 and CRY2olig-mCh were obtained from addgene (22852 & 60032) (Cambridge, MA, USA). The original iLID plasmids along with a truncated Tiam1(64-437) and ITSN1(1159-1509) were also ordered from addgene (60411, 60417, 60419). EB3-GFP was a kind gift by Niels Galjart.

All new membrane-tethered constructs were created with pClontech-eGFP-C1 vectors as backbone[43]. First of all the LOV-ssrA fusion domain of the iLID system was amplified with forward primer 5'-GATGAATTCAGCATGGGGGAGTTTCTGG-3' and reverse primer 5'-CATGGTACCAAAGTAATTTTCGTCGTTCGC-3' and ligated in the aforementioned vector through EcoRI and Acc65I restriction sites. The first C2 domain was cut with BsrGI and EcoRI from its original vector and inserted after eGFP. The second C2 domain was first amplified with forward primer 5'-CCTTCCGGAAGTAGTTGCACTGAACCCCTAGGC-3' and reverse primer

5’-CTAGATCTAAGCTTACCACAGCCCAGCAGCTCCACTCG-3’ before being cut and ligated with BspEI and BglII. The third C2 was amplified with forward primer 5’-GGTAAGCTTGGATCTTGCACTGAACCCCTAGGC-3’ and reverse primer 5’-CAAGATCTTCCGGTACCACAGCCCAGCAGCTCCAC-3’ and subsequently cut with HindIII and BglII to be inserted. One of three domains were added to the N-terminus of the eGFP-2xC2-iLID construct, EB3 was inserted with NheI and XhoI cuts after amplification with forward primer 5’-CATGCTAGCATGGCCGTCAATGTGTACTC-3’ and reverse primer 5’-CATCTCGAGGTACTCGTCCTGGTCTTC-3’. A second LOV-ssrA domain was ligated in through NheI and AgeI restriction sites after amplification with forward primer 5’-CTAGCTAGCATGGGGGAGTTTCTGGCAACC-3’ and reverse primer 5’-GGACCGGTCCAAAGTAATTTTCGTCGTTCG-3’. The PHR domain of CRY2 was amplified with forward primer 5’-CCTGCTAGCATGAAGATGGACAAAAAGAC-3’ and reverse primer 5’-GTACTCGAGCCAGCTATCCGCCACAATTTCATCCGGTGCTGCTCCGATCATGATCTGTGC-3’ to introduce the PDEIVADSW amino acid sequence at its C-terminus in order to recreate CRY2clust, which improves induced oligomerization[22] and was subsequently cut with NheI and XhoI for insertion.

All cytosolic constructs were cloned into pClontech-N1 vectors, starting with inserting mScarlet through AgeI and BsrGI restriction sites. The tandem repeats of sspB domains from single to quadruple insert were created through subsequent amplification and ligation of sspB with forward primer 5’-CATGGATCCATGGGACTCAGATCTCGAGCTC-3’ & reverse primer 5’-CCTACCGGTGGACCAATATTCAGCTCGTC -3’ cut with BamHI & AgeI, then with forward primer 5’-CATGGTACCATGGGACTCAGATCTCGAGCTC-3’ & reverse primer 5’-CGTGGATCCACCAATATTCAGCTCGTCATAG-3’ cut with Acc65I & BamHI, next with forward primer 5’-CATGTACAAGGGACTCAGATCTCGAGCTCAAGC-3’ & reverse primer 5’-CATCAATTGTATTTCCGGACCTGCAGGGTCAGGCCGCTCAG-3’ cut with BsrGI & MfeI, and finally with forward primer 5’-CATGCTAGCATGGGACTCAGATCTCGAGCTC-3’ & reverse primer 5’-CAGGGTACCACCAATATTCAGCTCGTCATAG-3’ cut with NheI & Acc65I. Fusion constructs of GEFs and the triple sspB repeat vector were made by amplifying Tiam1 with forward primer 5’-CATTCCGGAATATGCGACAGCTGTCGGATGCG-3’ & reverse primer 5’-CATCAATTGTCAGAATTCTTCCGTTTTGAGGAGC-3’ and ITSN1 with forward primer 5’-CATTCCGGAATATGTTGACCCCAACTGAAAGAAAGCG-3’ & reverse primer 5’-CATCAATTGTTAACCGAATTCCTTCTTTTTCTCAGTCTC-3’ before inserting them into the vector with BspEI & MfeI restriction sites. The active domain of 5-Phosphatase(214-644) was inserted into both the single and triple sspB repeat vector through the same BspEI & MfeI restriction sites after amplification with forward primer 5’-CATTCCGGAATATGTCGGATCTTGCAGACTACAAGC-3’ & reverse primer 5’-GTACAATTGTCAAGAAACGGAGCAGATGGTGC-3’

Cell culture & transfection

Human embryonic kidney cells (Hek293, American Type Culture Collection crl-1573) and human HeLa cervical cancer cells (ccl-2) were cultured in Dulbecco’s modified Eagle medium (DMEM) supplemented with Glutamax and 10% fetal bovine serum at 37°C and 7% CO_2. All cell culture media were obtained from Invitrogen (Breda, NL). For experiments, all cells were cultured on 25mm glass coverslips (Menzel- Gläser, Braunschweig, Germany) and transiently transfected with plasmids using 1µg/ml polyethylenimine approximately 18h prior to imaging. Hek293 cells were serum starved for 4h before experiments. Right

before imaging the culture medium was replaced with microscopy medium (137 mM NaCL, 5.4mM KCL, 1.8 mM $CaCL_2$, 0.8mM $MgCl_2$, 20mM glucose, and 20mM HEPES at PH = 7.4).

Confocal Laser Scanning Microscopy

All experiments were performed on an inverted Zeiss LSM510 meta confocal microscope (Carl Zeiss MicroImaging, Jena, Germany). Samples were imaged at room temperature using a 63x Plan-Apo/1.4 NA oil immersion objective. EGFP was excited with a 488nm argon laser line, and mScarlet using a 543nm helium-neon laser line.

Local optogenetic activation (Fig3e-g, Fig4) was achieved by scanning an ROI as represented on each relevant image with a 488nm laser line at 40 µW per pixel. Blue light illumination occurred every 20s unless only a single activation pulse was required. Total duration of the blue light pulses were approximately 5s with 3,2µs pixel dwell time. Optogenetic activation of entire cells was performed with an external 470 nm LED at 2-3 mW. Pulses of 5s were repeated every 20s unless only a single activation pulse was required.

For the iFRAP experiments (Fig1e, Fig2d-e) everything but a square ROI of 13 by 13 µm was bleached in laser scanning bleach mode with the 488nm laser at full power (30mW). Example images of iFRAP (Fig1f-h) were bleached in the same way but with a rectangular ROI of 13 by 26 µm across the entire cell to better demonstrate the effect. The bleaching occurred every 8s for a total duration of 2s and 3,2µs per pixel.

Data analysis

Raw microscopy images were analyzed using ImageJ (National Institutes of Health, Bethesda, MD). First a custom background correction macro was applied to all image stacks. The iFRAP (Fig1e, Fig2d-e) and dissociation (Fig3d) graphs were then obtained by plotting the intensities within the ROIs over time, normalizing the initial values to 1, and averaging all traces. Halftime values were extrapolated from the iFRAP curves and represented with a 95%-confidence interval calculated by the following equation: $\bar{x} \pm Z_{95/2} * \sigma/\sqrt{(n)}$, where Z refers to the Standard Normal statistical Z-table, σ is the standard deviation, and n the number of samples . Local membrane translocation (Fig3e-g) was visualized by subtracting the average baseline intensities from the post-translocation images in order to increase the visual contrast. We subsequently marked areas with intensities above the mean values within the ROI at t=0s post baseline substraction, in order to represent the minimal area to which translocated molecules diffuse. Representations of membrane deformation (Fig4a-b) were made by creating binary images through applying a threshold on the pre-activated and activated condition, where the difference in cell outline is then highlighted as blue for expansions and red for contractions.

List of Abbreviations

AsLOV2	Avena sativa Light-Oxygen-Voltage-sensing domain 2
Cdc42	Cell division control protein 42 homolog
CI	Confidence interval
CRY2	Cryptochrome Circadian Regulator 2
DH/PH	DbI-Homology/Pleckstrin-Homology
EB3	End-Binding protein 3
GEF	Guanine Exchange Factor
HEK	Human Embryonic Kidney
HEPES	N-2-hydroxyethylpiperazine-N-ethanesulfonic acid
ICAM-1	Intercellular Adhesion Molecule 1
iFRAP	inverse Fluorescence Recovery After Photobleaching
iLID	improved Light-Induced Dimer
ITSN1	Intersectin 1
MT	Microtubule
PM	Plasmamembrane
ROI	Region of Interest
SspB	Stringent starvation protein B
TEM	Trans-endothelial migration
Tiam1	T-lymphoma invasion and metastasis-inducing protein 1

Acknowledgements

This work is part of the research program ‘Spatio-temporal patterns of membrane protein activity’ with project number A-34, which is financed by the Netherlands Organization for Scientific Research (NWO).

Author contributions

O.G. and T.G. conceived and planned the experiments. O.G. and R.H. performed the experimental work. O.G. and T.G. wrote the manuscript.

References

1. Hancock JF, Robert G. Ras plasma membrane signalling platforms. Biochemical Journal. 2005;389(1):1-11.
2. Wickström SA, Fässler R. Regulation of membrane traffic by integrin signaling. Trends in cell biology. 2011;21(5):266-273.
3. Cho W, Stahelin RV. Membrane-protein interactions in cell signaling and membrane trafficking. Annu Rev Biophys Biomol Struct. 2005;34:119-151.
4. Weitzman M, Hahn KM. Optogenetic approaches to cell migration and beyond. Current opinion in cell biology. 2014;30:112-120.
5. Repina NA, Rosenbloom A, Mukherjee A, et al. At light speed: advances in optogenetic systems for regulating cell signaling and behavior. Annual review of chemical and biomolecular engineering. 2017;8:13-39.
6. Zhang K, Cui B. Optogenetic control of intracellular signaling pathways. Trends in biotechnology. 2015;33(2):92-100.
7. Goedhart J, van Unen J. Molecular perturbation strategies to examine spatiotemporal features of Rho GEF and Rho GTPase activity in living cells. Small GTPases. 2017:1-9.
8. Zimmerman SP, Asokan SB, Kuhlman B, et al. Cells lay their own tracks–optogenetic Cdc42 activation stimulates fibronectin deposition supporting directed migration. J Cell Sci. 2017;130(18):2971-2983.
9. Guntas G, Hallett RA, Zimmerman SP, et al. Engineering an improved light-induced dimer (iLID) for controlling the localization and activity of signaling proteins. Proceedings of the National Academy of Sciences. 2015;112(1):112-117.
10. Strickland D, Lin Y, Wagner E, et al. TULIPs: tunable, light-controlled interacting protein tags for cell biology. Nature methods. 2012;9(4):379.
11. Wagner E, Glotzer M. Local RhoA activation induces cytokinetic furrows independent of spindle position and cell cycle stage. J Cell Biol. 2016:jcb. 201603025.
12. Goodwin JS, Drake KR, Remmert CL, et al. Ras diffusion is sensitive to plasma membrane viscosity. Biophysical journal. 2005;89(2):1398-1410.
13. Lommerse PH, Vastenhoud K, Pirinen NJ, et al. Single-molecule diffusion reveals similar mobility for the Lck, H-ras, and K-ras membrane anchors. Biophysical journal. 2006;91(3):1090-1097.

14. Silvius JR, Bhagatji P, Leventis R, et al. K-ras4B and prenylated proteins lacking “second signals” associate dynamically with cellular membranes. Molecular biology of the cell. 2006;17(1):192-202.

15. Pudasaini A, El-Arab KK, Zoltowski BD. LOV-based optogenetic devices: light-driven modules to impart photoregulated control of cellular signaling. Frontiers in molecular biosciences. 2015;2:18.

16. Ouyang M, Sun J, Chien S, et al. Determination of hierarchical relationship of Src and Rac at subcellular locations with FRET biosensors. Proceedings of the National Academy of Sciences. 2008;105(38):14353-14358.

17. Benedetti L, Barentine AE, Messa M, et al. Light-activated protein interaction with high spatial subcellular confinement. Proceedings of the National Academy of Sciences. 2018:201713845.

18. Ho KKY, Murray V, Lee JW, et al. Coupling the Increase in Membrane Tension and the Synthesis of Phosphatidylserine in a “Smart” Artificial Cell. Biophysical Journal. 2015;108(2):465a.

19. Li H, Sineshchekov OA, Wu G, et al. In vitro activity of a purified natural anion channelrhodopsin. Journal of Biological Chemistry. 2016;291(49):25319-25325.

20. Andersen MH, Graversen H, Fedosov SN, et al. Functional analyses of two cellular binding domains of bovine lactadherin. Biochemistry. 2000;39(20):6200-6206.

21. Dundr M, Hoffmann-Rohrer U, Hu Q, et al. A kinetic framework for a mammalian RNA polymerase in vivo. Science. 2002;298(5598):1623-1626.

22. Park H, Kim NY, Lee S, et al. Optogenetic protein clustering through fluorescent protein tagging and extension of CRY2. Nature communications. 2017;8(1):30.

23. Zayner JP, Sosnick TR. Factors that control the chemistry of the LOV domain photocycle. PLoS One. 2014;9(1):e87074.

24. Hauser G, Seiffert S, Oppermann W. Systematic evaluation of FRAP experiments performed in a confocal laser scanning microscope–Part II: Multiple diffusion processes. Journal of microscopy. 2008;230(3):353-362.

25. Saffman PG, Delbrück M. Brownian motion in biological membranes. Proceedings of the National Academy of Sciences. 1975;*72*(8):3111-3113.

26. Busch KE, Brunner D. The microtubule plus end-tracking proteins mal3p and tip1p cooperate for cell-end targeting of interphase microtubules. Current Biology. 2004;14(7):548-559.

27. Akhmanova A, Steinmetz MO. Tracking the ends: a dynamic protein network controls the fate of microtubule tips. Nature reviews Molecular cell biology. 2008;9(4):309.

28. Furuya A, Kawano F, Nakajima T, et al. Assembly domain-based optogenetic system for the efficient control of cellular signaling. ACS synthetic biology. 2017;6(6):1086-1095.

29. Michaelson D, Silletti J, Murphy G, et al. Differential localization of Rho GTPases in live cells: regulation by hypervariable regions and RhoGDI binding. The Journal of cell biology. 2001;152(1):111-126.

30. Minard ME, Herynk MH, Collard JG, et al. The guanine nucleotide exchange factor Tiam1 increases colon carcinoma growth at metastatic sites in an orthotopic nude mouse model. Oncogene. 2005;24(15):2568.

31. Garcia-Mata R, Boulter E, Burridge K. The'invisible hand': regulation of RHO GTPases by RHOGDIs. Nature reviews Molecular cell biology. 2011;12(8):493.

32. Kraynov VS, Chamberlain C, Bokoch GM, et al. Localized Rac activation dynamics visualized in living cells. Science. 2000;290(5490):333-337.

33. Das S, Yin T, Yang Q, et al. Single-molecule tracking of small GTPase Rac1 uncovers spatial regulation of membrane translocation and mechanism for polarized signaling. Proceedings of the National Academy of Sciences. 2015;112(3):E267-E276.

34. Castro-Castro A, Muriel O, del Pozo MA, Bustelo XR. Characterization of novel molecular mechanisms favoring Rac1 membrane translocation. PloS one. 2016;11(11):e0166715.

35. Mertens AE, Roovers RC, Collard JG. Regulation of Tiam1–Rac signalling. FEBS letters. 2003;*546*(1):11-16.

36. Heemskerk N, van Rijssel J, van Buul JD. Rho-GTPase signaling in leukocyte extravasation: an endothelial point of view. Cell adhesion & migration. 2014;8(2):67-75.

37. Van Buul JD, Allingham MJ, Samson T, et al. RhoG regulates endothelial apical cup assembly downstream from ICAM1 engagement and is involved in leukocyte trans-endothelial migration. J Cell Biol. 2007;178(7): 1279-1293.

38. van Rijssel J, Kroon J, Hoogenboezem M, et al. The Rho-guanine nucleotide exchange factor Trio controls leukocyte transendothelial migration by promoting docking structure formation. Molecular biology of the cell. 2012;23(15): 2831-2844.

39. ten Klooster JP, Evers EE, Janssen L, et al. Interaction between Tiam1 and the Arp2/3 complex links activation of Rac to actin polymerization. Biochemical Journal. 2006;397(1):39-45.

40. Connolly BA, Rice J, Feig LA, et al. Tiam1-IRSp53 complex formation directs specificity of rac-mediated actin cytoskeleton regulation. Molecular and cellular biology. 2005;25(11):4602-4614.

41. Wu YI, Frey D, Lungu OI, et al. A genetically encoded photoactivatable Rac controls the motility of living cells. Nature. 2009;461(7260):104.

42. Dagliyan O, Tarnawski M, Chu P-H, et al. Engineering extrinsic disorder to control protein activity in living cells. Science. 2016;354(6318):1441-1444.

43. Kremers G-J, Goedhart J, van den Heuvel DJ, et al. Improved green and blue fluorescent proteins for expression in bacteria and mammalian cells. Biochemistry. 2007;46(12):3775-3783.